33RD INTERNATIONAL COSMIC RAY CONFERENCE, RIO DE JANEIRO 2013
THE ASTROPARTICLE PHYSICS CONFERENCE

Measurement of the Cosmic Ray Energy Spectrum with IceTop 73

THE ICECUBE COLLABORATION[1].

[1] *See special section in these proceedings*

bahtiyar@udel.edu

Abstract: We report on the measurement of the all particle cosmic ray energy spectrum with the IceTop air shower array in the energy range from 1.6 PeV up to 1.3 EeV. The IceTop air shower array is the surface component of the IceCube Neutrino Observatory at the geographical South Pole. The analysis was performed using IceTop in its 73 station configuration when it was 90% complete. The spectrum was derived using an iterative unfolding with shower size as an energy proxy.

Corresponding authors: Bakhtiyar Ruzybayev[1], Javier Gonzalez[1]
[1] *University of Delaware*

Keywords: IceTop, All-particle energy spectrum.

1 Introduction

High resolution measurements of the cosmic ray energy spectrum and the elemental composition will improve our understanding of the acceleration and propagation of high energy cosmic rays. In this paper we investigate the spectrum in the region from 1.6 PeV up to 1.3 EeV. We are reporting on the measurement of the spectrum by the IceTop air shower array in its 73 station configuration using the shower size for the energy estimation. The shower size to energy conversion is performed assuming a mixed primary composition as described in reference [1] and is referred to as H4a model. The zenith dependence of the shower attenuation is used for estimating the uncertainty on the flux due to primary composition.

2 The IceTop Detector and Data

IceTop [2] is the surface component of the IceCube Neutrino Observatory. IceTop is designed to detect air showers from primary cosmic rays in the 300 TeV to 1 EeV energy range. IceTop is an air shower array consisting of 81 surface stations in its final configuration and covering an area of one square kilometer. The inter-station separation is about 125 m. Each station consists of two ice Cherenkov tanks separated by 10 m. Two Digital Optical Modules (DOM) [3] are deployed per tank. Each DOM contains a 10 inch photomultiplier tube (PMT) and electronics for signal processing and readout [4]. An Ice-Top station is considered triggered when both tanks in the station record hits within 1 μs of each other. DOM charges are calibrated using signals from single muons and all charges are converted to the tank and DOM independent unit of 'Vertical Equivalent Muon' (VEM) [2].

This analysis was done on the data taken in the period from June 1, 2010 to May 13, 2011 when IceTop consisted of 73 stations. The effective live-time of the data-set used is 327 days.

3 Simulation

Detailed simulations were used to relate measured air shower parameters to the properties of primary cosmic rays. Air showers were simulated in a wide energy range from 10^5 GeV to $10^{9.5}$ GeV with CORSIKA [6]. Showers above 10^8 GeV were 'thinned' [7] to reduce computational time and storage volume. Hadronic interaction models used were SIBYLL 2.1 [8] for interactions with energies greater than 80 GeV and FLUKA [9] at lower energies. A smaller set was simulated using QGSJET-II [10] for systematic studies. Simulated atmosphere had an atmospheric overburden of 692.9 g/cm^2 (680 hPa), which is also the average overburden for the full year of data. Snow cover on top of tanks in simulation was same as measured in February, 2010. Air showers were simulated with equal number of showers per $\sin\theta\cos\theta$ bin, in a zenith range of 0 to 40 degrees. Four primary types, H, He, O, Fe, were simulated with more than 42000 CORSIKA showers per primary. During the analysis showers are reweighted by different assumed spectra. Each CORSIKA shower was resampled 100 times to increase statistics. Shower cores were uniformly distributed over areas larger than the detector area with an energy dependent resampling radius. The detector response was simulated using IceCube software that simulates the entire chain of data taking and all the hardware [2]. Interactions of charged particles with the IceTop tanks were simulated using the GEANT4 [11] package. The simulations of single primary elements were weighted by a power law spectrum, $\frac{dN}{dE} \propto E^{-2.7}$. For a mixed composition we used the model from reference [1], referred to as H4a. The H4a model consists of 5 elemental groups.

4 Analysis

4.1 Basic reconstructions

The IceTop reconstruction algorithm [2] uses information from individual tanks, including location, charge and pulse time. Shower direction, core location and shower size are reconstructed by fitting the measured charges with a Lateral Distribution Function (LDF) and the signal times with a

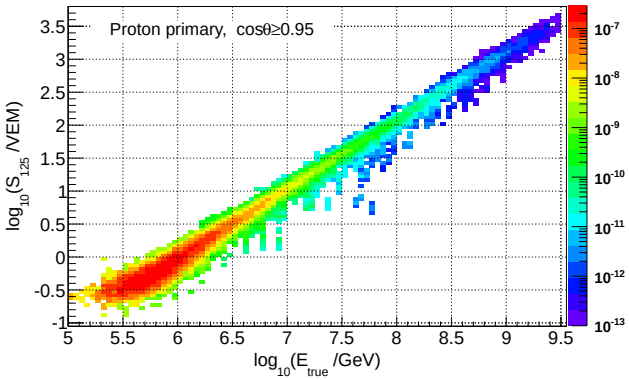

Fig. 1: $\log_{10}(S_{125})$ vs. $\log_{10}(E_{true})$. scatter plot for proton primary simulation with $\cos\theta \geq 0.95$, weighted by a flux model $\frac{dN}{dE} \propto E^{-2.7}$

function describing the geometric shape of the shower front. The lateral distribution function is defined as:

$$S(R) = S_{ref}\left(\frac{R}{R_{ref}}\right)^{-\beta-0.303\log_{10}\left(\frac{R}{R_{ref}}\right)}, \qquad (1)$$

where S_{ref} is the shower size or signal at a reference distance R_{ref} to the shower axis, β is the slope of the logarithmic LDF at R_{ref}. The shower front is described using the signal times as:

$$t(\mathbf{x}) = t_0 + \frac{1}{c}(\mathbf{x}-\mathbf{x}_c)\mathbf{n} + \Delta t(R), \qquad (2)$$

where $t(\mathbf{x})$ is the signal time of the tank at position $\mathbf{x}$, $\mathbf{x}_c$ is the position of shower core on the ground and $\mathbf{n}$ is the unit vector in the direction of movement of the shower. The functional form of $\Delta t(R)$ is a sum of a parabola and a gaussian which describes the curvature as a deviation from the plane perpendicular to the shower axis containing $\mathbf{x}_c$. Equations 1 and 2 describe the expectations for the charge and time of air shower signals. They are fitted to the measured data using a maximum likelihood method [2] with an additional term describing the saturation likelihood. The shower size, S_{125}, is defined as the fitted value of the LDF (Eq.1) at a perpendicular distance of 125 m away from the shower axis. From this fit we get the reconstrcuted core location (x,y), zenith (θ) and azimuthal (ϕ) angles.

Snow accumulates on top of IceTop tanks with time, which reduces the measured signal in a tank. To correct for this reduction, the expected signal in the likelihood fitting procedure is reduced according to:

$$S_{expected,corrected} = S_{expected}\exp\left(-\frac{d\sec\theta}{\lambda}\right), \qquad (3)$$

where d is the snow on top of the tank, θ is the measured zenith angle of the shower and $\lambda = 2.1$ m is the effective attenuation length of the electromagnetic component of the shower in the snow.

The core resolution of the current reconstruction method is better than 15 m around few PeV and improves to less than 8 m at higher energy. The directional resolution is between $0.2^\circ - 0.8^\circ$, depending on energy and zenith angle.

Table 1: Fit parameters for Eq.4 for the mixed, H4a, composition assumption in four zenith ranges.

Composition	Zenith range	$\mathbf{p}_0$	$\mathbf{p}_1$
H4a	$\cos\theta \geq 0.95$	6.018	0.938
	$0.95 > \cos\theta \geq 0.90$	6.062	0.929
	$0.90 > \cos\theta \geq 0.85$	6.117	0.921
	$0.85 > \cos\theta \geq 0.80$	6.182	0.914

4.2 Event selection

The event selection was done according to the following cuts which were applied both to the simulated and the experimental data.

1. Events must trigger at least 5 stations with reconstructed fits converged (Eqs.1 and 2).
2. Events with $\log_{10}(S_{125}/\text{VEM}) \geq 0.0$.
3. Events with $\cos\theta \geq 0.8$ are selected.
4. Reconstructed cores must be within a geometric boundary that is inside the outermost stations.
5. Events with the largest signal in a station on the edge of the array are rejected.
6. Events in which no station has a signal greater than 6 vertical equivalent muons are rejected.

The last two cuts were introduced to reduce migration of high energy showers that fall outside the geometric containment but still trigger a large number of stations and get reconstructed within the containment area.

4.3 Energy estimation method

To estimate the energy of the primary cosmic ray, we use the relationship between shower size S_{125} and the true primary energy, E_{true}, from simulations. This relationship depends on the mass of the primary particle and the zenith angle of the air shower. Figure 1 shows a 2-dimensional histogram of the $\log_{10}(S_{125})$ vs $\log_{10}(E_{true})$ for simulated protons weighted by a flux model $\frac{dN}{dE} \propto E^{-2.7}$. For a given zenith bin we slice the distribution shown in Fig.1 in 0.05 bins of $\log_{10}(S_{125})$ and plot the distributions of true energy for each bin. We fit each energy distribution with a gaussian function and use the fitted mean as the energy estimate for the given bin of $\log_{10}(S_{125})$. The relationship between $\log_{10}(S_{125})$ and $\log_{10}(E_{true})$ is:

$$\log_{10}(E) = p_1\log_{10}(S_{125}) + p_0. \qquad (4)$$

Table 1 shows the fit parameters for the mixed compositon assumption. For each composition assumption we get a set of energy estimators as shown in figure 2 for the H4a model assumption. When showing spectra for a given zenith range and assumed composition, the energy was estimated with the appropriate functional relationship.

4.4 Flux derivation

The flux was calculated according to the following formula:

$$\mathrm{J}(E) = \frac{\mathrm{d}N}{\mathrm{d}E\,A_{eff}\,\Delta\Omega\,T}, \qquad (5)$$

where $\Delta\Omega = 2\pi(\cos\theta_{min} - \cos\theta_{max})$, solid angle range, T = live-time, and A_{eff} is the effective area

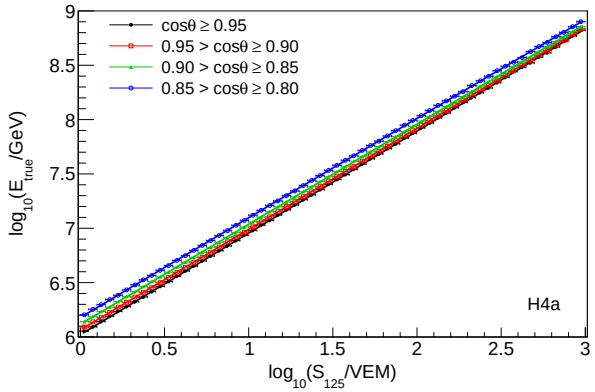

Fig. 2: S_{125}-to-E_{true} relations in four zenith ranges for the H4a composition assumption.

$$A_{eff} = \mathrm{A_{cut}} \frac{\cos\theta_{max} + \cos\theta_{min}}{2} \varepsilon(E), \qquad (6)$$

where $\mathrm{A_{cut}}$ is the geometric containment and $\varepsilon(E)$ is the detector efficiency

$$\varepsilon(E) = \frac{N_{reco}}{N_{true}}. \qquad (7)$$

where N_{reco} is the number of events with reconstructed energy and zenith angle within the bin, and reconstructed core contained in the IceTop fiducial area, and N_{true} is the number of events with true energy and true zenith angle within the bin, and true core contained in the IceTop fiducial area. Efficiencies were evaluated and applied separately for each composition assumption and each of the four zenith bins. Examples of the derived spectra for different composition assumptions in four zenith ranges can be seen in Fig.3.

The final spectrum was derived assuming the H4a model and averaging over the full zenith range $\cos\theta \geq 0.8$. The spectrum was unfolded by an iterative procedure in which the spectrum derived in the previous step was used to determine the effective area and the S_{125}-to-E_{true} relation for the next spectrum evaluation. In case of convergence the effective area effectively accounts for migrations due to finite resolutions. In the first step the spectrum was derived assuming the H4a model. The result was fitted by the sum of three power-law functions each with an exponential cutoff. The fitted spectrum, keeping the fractional contributions of the elemental groups as in the H4a model, was used for the simulation of the next step efficiencies and energy conversions. The spectrum derived in this first iteration step showed no significant difference to the one derived using the original H4a model meaning that the iterative unfolding converged already after one iteration. The same algorithm was applied starting with a featureless power-law spectrum with an H4a composition. In this case the spectrum converged after two iterations.

4.5 Systematics

There are four major systematic uncertainties on energy estimation that were accounted for in this analysis. All systematic uncertainties on primary energy were propagated to flux. When calculating different systematics, all conditions except the systematics under investigation, are kept the same.

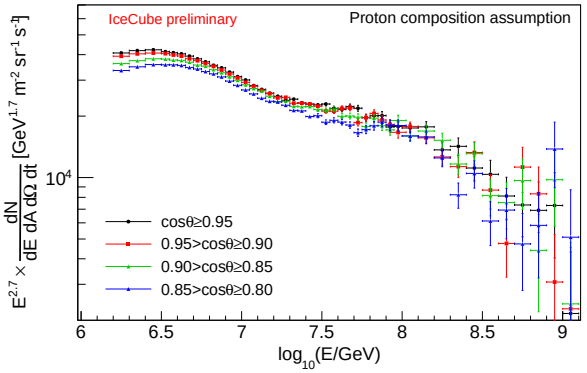

(a) Proton.

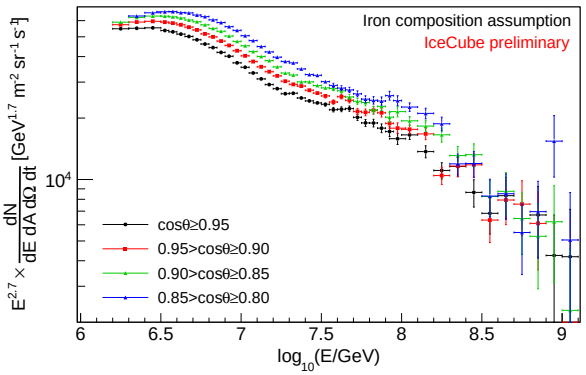

(b) Iron.

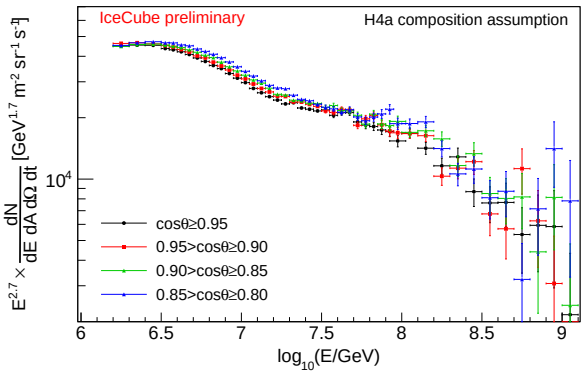

(c) H4a.

Fig. 3: Cosmic ray energy spectrum for 3 composition assumptions and 4 zenith ranges.

Uncertainty in VEM calibration

The measured charge of each IceTop tank is calibrated using the signal due to atmospheric muons [2]. From simulation studies a 3% uncertainty on the charge callibration and thus on the absoulute energy scale was found [5]. This uncertainty on absolute charge calibration translates into an absolute uncertainty in the signal, S_{125}, and consecutively in the energy. We propagate this uncertainty to primary energy and flux.

Uncertainty in snow correction
The systematic error due to snow correction arises from the uncertainty in the correction parameter λ. In the analysis we used λ =2.1 m and the uncertainty is $\pm$0.2 m. The error in S_{125} is estimated from the difference between shower size spectra derived using $\lambda = 1.9$ m and $\lambda = 2.3$ m. This error is propagated to an error in energy using the same S_{125}-to-E_{true} conversion (Eq.4) for all three S_{125} spectra.
Difference between SYBILL 2.1 and QGSJET II
To compare two interaction models, S_{125}-to-E_{true} relations were recalculated using the smaller simulated sets with QGSJET II as the interaction model. Comparison of the S_{125}-to-E_{true} relations show that for a given S_{125}, QGSJET II simulation results in lower energies compared to SYBILL 2.1. The largest difference is $\Delta\log(E/\mathrm{GeV}) = 0.02$, meaning that for the same primary energy QGSJET produces larger S_{125} signal compared to SYBILL 2.1.
Uncertainty and composition dependence
The method used in this analysis requires a predefined composition assumption to translate the measured S_{125} spectrum to the primary energy spectrum. In addition to the baseline scenario, the mixed composition H4a, we considered 4 differnet composition assumptions (pure proton, pure helium, pure oxygen and pure iron), to estimate the impact of the composition uncertainties to the all-particle spectrum.

Assuming that the cosmic ray directions are isotropically distributed, the measurement of the spectrum in different zenith ranges should yield the same result for each zenith. For a given energy, protons or light nuclei penetrate deeper into the atmosphere compared to heavy nuclei like iron. Heavy nuclei start to interact higher in the atmosphere and showers will be at a different stage of development at the detector level compared to the light nuclei. When looking at large zenith angle events, one effectively increases the amount of atmosphere that showers need to traverse to get to the detector. This information is sensitive to composition.

Reconstruction of the experimental data assuming pure proton and pure iron compositions in four zenith ranges are shown in Figs. 3(a) and 3(b). It can be seen that for a pure proton assumption the most inclined spectrum ($0.80 \leq \cos\theta < 0.85$) is systematically lower than vertical spectrum ($\cos\theta \geq 0.95$), in the energy range where statistics are not an issue. While for pure iron assumption it is the opposite, the inclined spectrum is systematically higher than vertical.

Four zenith spectra for the mixed, H4a, composition assumption can be seen in Fig. 3(c). Compared to pure proton and pure iron , H4a assumption leads to a smaller difference between vertical and inclined spectra, but still not zero. To estimate the systematic uncertainty in the all-particle energy spectrum due to composition, we use the differences for the H4a assumption between the final (Eq.5 with $\cos\theta_{min} = 1.0$, and $\cos\theta_{max} = 0.8$) and the vertical ($\cos\theta \geq 0.95$) spectra, and the final and the inclined ($0.80 \leq \cos\theta < 0.85$) spectra in the energy range $6.2 < \log_{10}(E/\mathrm{GeV}) < 7.5$ where statistical fluctuations are negligible. The largest difference between spectra is taken as a fixed value for the error due to composition across all energies as a conservative estimate.

5 Results and discussion

The final spectrum is shown in Fig.4. The IceTop Shower Size parameter, S_{125}, is calibrated against the true primary energy using the H4a composition model as an input to our simulations. We observe that, beyond our systematics, the all-particle cosmic-ray energy spectrum does not follow a single power law above the knee (4.4 ± 0.4 PeV), but shows significant structure. The final spectrum was fitted by a simple power functions of the form

$$\frac{\mathrm{d}N}{\mathrm{d}\ln E\,\mathrm{d}A\,\mathrm{d}\Omega\,\mathrm{d}t} = I_0 \left(\frac{E}{1\,\mathrm{GeV}}\right)^{-\gamma+1}, \qquad (8)$$

in four different energy ranges. The break points in the spectrum are defined as the intersection of the fitted power functions.

The spectral index before the knee is $-2.63 \pm 0.01 \pm 0.06$, and changes smoothly between 4 to 7 PeV to $-3.13 \pm 0.01 \pm 0.03$. Another break is observed at around 18 ± 2 PeV, above which the spectrum hardens with a spectral index of $-2.91 \pm 0.01 \pm 0.03$. A sharp fall is observed beyond 130 ± 30 PeV with a spectral index of $-3.37 \pm 0.08 \pm 0.08$. The power function fits to the spectrum and their parameters are shown in Fig.4.

In summary, we have obtained a measurement of the cosmic-ray energy spectrum with an energy resolution of 20% below 10 PeV and less than 13% above 10 PeV. Systematic uncertainty is the main error on flux and is no more than $\pm$9%. The hardening of the spectrum around 18 PeV and steepening around 130 PeV is a clear signature of the spectrum and can not be attributed to any of the systematics or detector artefacts.

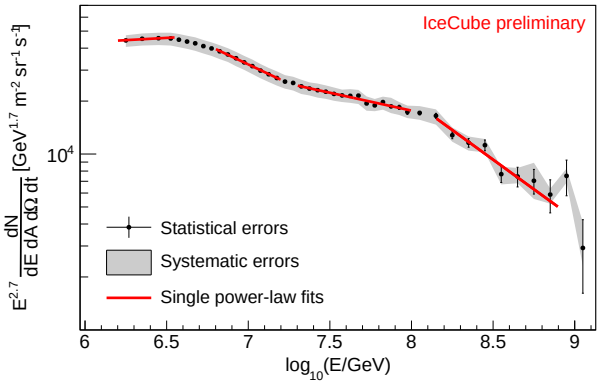

Fig. 4: Spectral fits in different energy ranges. Shaded area represents the systematic errors added in quadrature.

Acknowledgment: The ICRC 2013 is funded by FAPERJ, CNPq, FAPESP, CAPES and IUPAP.

References

[1] T.K.Gaisser, Astropart. Phys. 35 (2012) 801-806
[2] R.Abbasi et al, Nucl. Instrum. Meth. A 700 (2013) 188-220
[3] R.Abbasi et al, Nucl. Instrum. Meth. (2009) 294-316
[4] R.Abbasi et al, Nucl. Instrum. Meth. (2010) 139-152
[5] A. Van Overloop, Proc. of the 32nd ICRC, Beijing (2011)
[6] D.Heck et al, report FZKA 6019 (1998)
[7] D.Heck, T.Pierog, `http://www-ik.fzk.de/corsika/usersguide/corsika_tech.html`
[8] E.Ahn et al, Physics Review D 80 (2009) doi:10.1103/PhysRevD.80.094003
[9] G.Battistoni et al, AIP Conf. Proc. 896 (2007) 31-49
[10] S.Ostapchenko, Nucl. Phys. B Proc. Suppl 151 (2006) 143-146
[11] S.Agostinelli et al, Nucl. Instrum. Meth A 506 (2003) 250-303